Title:

Remote Cortical Network for Frontal Cognitive Symptoms derived from Tau Accumulation in Progressive Supranuclear Palsy

Authors:

Yuki Hori[a], Hironobu Endo[a*], Kenji Tagai[a], Yuko Kataoka[a], Ryoji Goto[a], Shin Kurose[a], Yuki Momota[a], Naomi Kokubo[a], Chie Seki[a], Sho Moriguchi[a], Hitoshi Shimada[b], Hitoshi Shinotoh[a], Takahiko Tokuda[a], Keisuke Takahata[a], Takafumi Minamimoto[a], Makoto Higuchi[a], and Toshiyuki Hirabayashi[a*]

Affiliations:

[a] Advanced Neuroimaging Center, National Institutes for Quantum Science and Technology, 4-9-1 Anagawa, Inage-ku, Chiba 263-8555, Japan

[b] Center for Integrated Human Brain Science, Department of Functional Neurology & Neurosurgery, Niigata University, 1-757 Asahimachidori, Chuo-ku, Niigata 951-8585 Japan

[*] Authors to whom all correspondence should be addressed:

Toshiyuki Hirabayashi, Ph.D.

Advanced Neuroimaging Center, National Institutes for Quantum Science and Technology, 4-9-1 Anagawa, Inage-ku, Chiba 263-8555, Japan

E-mail: hirabayashi.toshiyuki@qst.go.jp

Hironobu Endo, M.D. Ph.D.

Advanced Neuroimaging Center, National Institutes for Quantum Science and Technology, 4-9-1 Anagawa, Inage-ku, Chiba 263-8555, Japan

E-mail: endo.hironobu@qst.go.jp

Abstract:
Progressive Supranuclear Palsy (PSP) is a neurodegenerative disorder characterized by movement impairments and frontal cognitive dysfunctions. While motor symptoms are linked with subcortical tau deposits, mechanisms underlying the frontal cognitive symptoms remain unclear due to limited tau accumulation in the frontal cortex and heterogeneous tau distribution. Here, we combined high-contrast tau PET with normative connectome to identify a common network extended from tau deposits underlying the frontal cognitive symptoms in PSP. Regions with tau deposition were connected to a common cortical network that was not detectable through atrophy-based analyses. This network was primarily overlapped with canonical action-mode and frontoparietal networks. While the degree of subcortical tau deposition or atrophy correlated with motor symptoms, only connectivity between tau deposition sites and the derived cortical network explained the frontal cognitive deficits. These findings propose network mechanisms underlying frontal cognitive impairments in PSP, emphasizing the role for remote effects of pathological tau deposits.

Main Text:

INTRODUCTION

Progressive supranuclear palsy (PSP) is a neurodegenerative disorder primarily characterized by movement impairments such as oculomotor deficits, postural instability, and akinesia [1-3]. In addition to these motor-related symptoms, PSP is frequently associated with cognitive deficits, especially those related to the frontal cortical dysfunctions [4,5]. Pathologically, PSP is known as a four-repeat tauopathy, where the aggregation of hyperphosphorylated tau proteins is implicated as a major cause of clinical symptoms, accompanied by neuroinflammation and atrophy. [6,7]. Tau lesions, neuronal loss and gliosis have been found in cortical and subcortical regions, including basal ganglia, midbrain, motor-related cortical areas, and cerebellum [8], and damages to these structures have been associated with motor dysfunctions and general disease severity [2,3,9,10]. Subcortical atrophy, especially in the midbrain and cerebellum, is another notable pathological hallmark of PSP patients, distinguishing them from the patients of Parkinson's disease or age-matched healthy controls. [11,12]. However, the mechanisms underlying the frontal cognitive decline in PSP remain elusive, as frontal lobe atrophy or tau deposition is rarely observed beyond the primary and supplementary motor areas [12-15].

Neurodegenerative diseases, including PSP, are increasingly conceptualized as network-based disorders [16]. The aggregation of pathological proteins in specific brain regions disrupts synaptic function, with damage propagating across interconnected networks. [17,18], and accelerating clinical symptoms [19]. In PSP, declined functional connectivity (FC) between the atrophied midbrain region and other areas including the frontal cortex has been reported for patients [20]. In addition, hypoperfusion [21,22] and hypometabolism [23,24] in the frontal cortex have been observed even in the absence of local pathological changes, suggesting that the frontal cognitive dysfunctions in PSP patients may result from the remote effects of subcortical pathologies.

Lesion network mapping (LNM) has emerged as a powerful approach to identify brain regions commonly connected from heterogeneous lesion sites associated with shared symptoms across stroke patients using normative connectome data. This approach is based on the principle that, while a lesion occurs in a specific brain region, it also causes indirect impairments in regions connected from the lesion sites. The LNM has uncovered hidden core regions associated with diverse symptoms across neurological conditions, including visual hallucinations [25], delusions [26], amnesia [27], loss of consciousness [28], criminal behavior [29], and abnormal movements such as freezing of gait and hemichorea-hemiballismus [30]. Recently, LNM has been extended to atrophy-based analyses [31], demonstrating its potential to identify common brain locations functionally connected

from atrophied regions, despite the heterogeneity of atrophy patterns among patients of Alzheimer's disease. Importantly, core regions identified through LNM have been shown to align with neuromodulation targets for symptom relief [32,33], further validating its utility.

In this study, we aimed to identify a common network responsible for frontal cognitive dysfunctions in PSP. Specifically, we investigated whether impairments in PSP could be attributed to local tau deposition or atrophy, or to their remote effects. Additionally, we sought to determine whether the remote effect is specific for frontal cognitive dysfunctions and whether remote effects of tau deposits differ from those of atrophy. To achieve this, we used a novel PET probe we recently developed, florzolotau (18F) (also known as PM-PBB3 or APN-1607) for detecting tau deposits [34]. This probe provides high metabolic stability and remarkable contrast at the single-patient level not only for Alzheimer's disease (AD), but also for non-AD tauopathies including PSP, which has been difficult with previous probes [35]. By applying network mapping to PET-detected tau deposits in individual patients, we identified common brain regions functionally connected with the locations of pathological tau aggregates, and examined their relationships with clinical symptoms (Fig. 1). Our results reveal the network mechanisms underlying frontal cognitive impairments in PSP and highlight the distinct contributions of remote effects mediated by tau deposits.

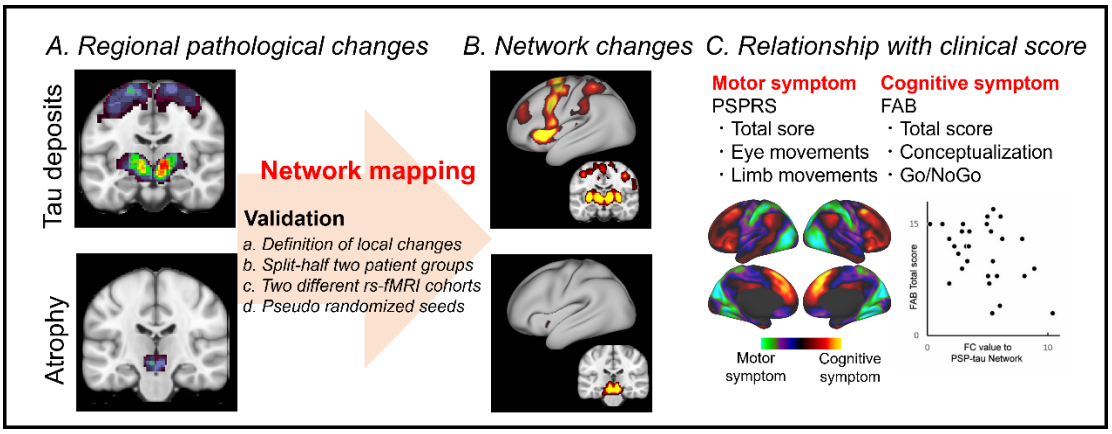

Fig. 1 Overview. Identification of the regional and network impairments responsible for the cognitive dysfunction in PSP. Regional impairments caused by the tau deposits and atrophy were identified by ^{18}F-florzolotau PET and MRI, respectively (A). Network impairments were identified using a resting-state functional MRI (rs-fMRI) database of healthy subjects and regional impairments as seeds (B). Finally, the relationship between clinical symptoms and a specific brain region or functional networks were determined (C). To validate this approach, we performed four evaluations; (a) comparison among the maps connected from impairment region calculated by different definition; (b) reproducibility evaluation using two-split half

groups; (c) comparison between the maps calculated by two different rs-fMRI cohorts, (d) comparison with the maps calculated by pseudo randomized seeds to exclude the possibility that it is simply hub regions in the brain irrespective of the locations of tau deposits or atrophy.

RESULTS

Localization of tau deposit and brain atrophy in individual PSP patients

We analyzed the data from 37 patients (22 males and 15 females) with PSP-Richardson syndrome, which represents the most typical clinical features of PSP [36]. The mean age and duration of the disease were 70 ± 1.2 years old and 3.4 ± 0.40 years (mean ± standard error of the mean), respectively. Disease severity, as assessed by the PSP rating scale (PSPRS), was 41 ± 2.9. All the patients exhibited tau deposits measured with florzolotau PET, without accumulation of amyloid-beta as determined with Pitsburgh compound-B (PiB) PET.

To identify the locations of tau deposition and atrophy, we first calculated *t*-score maps of florzolotau PET and MRI-based voxel-based morphometry (VBM) images for each patient. These maps were generated by comparing the patients' data with the corresponding images of age-matched healthy controls (N = 48) (Fig. 2). Tau deposits were most frequently observed across the patients subcortically in the globus pallidus (GP) ($p < 0.0003$, unpaired *t*-test) and midbrain ($p < 0.0006$), with 62 and 57% overlaps across patients when thresholded at $p = 0.001$, respectively (Fig. S1C). In addition, moderate accumulation of tau was also detected in motor-related cortical areas in the precentral gyrus ($p < 0.003$, 25% overlap). Meanwhile, brain atrophy was primarily localized in the midbrain ($p < 0.01$, 27% overlap), cerebellum ($p < 0.03$, 27%), and GP ($p < 0.05$, 14%) (Fig. S1B and D). Note that only a limited overlap of either tau deposition or atrophy was observed in the frontal cortex, except for a part of the primary/supplementary motor and premotor areas.

Common extended network derived from tau deposit or brain atrophy across PSP patients

Next, we sought to determine a common network functionally connected with locations of tau deposit and/or atrophy in PSP patients. We first examined where in the brain was functionally connected with the locations of tau deposit in each patient using a tau-network mapping approach (See Fig. S2). The locations of tau deposit in each patient were identified based on the *t*-score map ($p < 0.001$, one-sided, uncorrected). These locations were served as seed regions for calculating the whole-brain FC maps using a publicly available resting-state functional MRI (rs-fMRI) dataset of healthy subjects [Brain Genomics Superstruct Project (GSP) [37]] (N = 100 [25]). Although tau deposits were restricted to subcortical areas and some parts of motor-related cortices (Fig. 2A and C), a common network derived from tau deposits extended to more widespread cortical areas, including the lateral prefrontal cortex (lPFC), dorsal anterior cingulate cortex (dACC),

posterior parietal cortex (PPC), anterior insula (AI), in addition to subcortical areas with tau accumulation such as GP and midbrain ($p < 0.05$, family-wise error (FWE)-corrected; Fig. 3A and D). In contrast, atrophy network mapping—with thresholded ($p < 0.001$, uncorrected) atrophy maps of the same patients as seed regions—revealed an extended network largely restricted to subcortical areas, including the midbrain, pons, and a part of cerebellum (Fig. 3B and E). These results suggest that the extended, common cortical network observed in the PSP patients is specifically derived from tau deposits, rather than atrophy.

To validate these results, we conducted several control analyses. First, we confirmed that the obtained common network was basically conserved even when different thresholds ($p < 0.005$, uncorrected or $p < 0.05$, FWE corrected) were used to define the seed regions from the map of tau accumulation (Fig. S3A-F) and atrophy (Fig. S3G-L), suggesting that the results did not depend on a specific value of threshold for seed definition. Second, the reproducibility of the common cortical network was assessed by splitting the original dataset into two random subgroups. The resultant FC maps derived from tau deposit or atrophy were significantly correlated between the two subgroups (Fig. S4, $r = 0.87$ and 0.74, $p < 0.001$ for tau- and atrophy-network mapping, respectively). Third, to rule out connectome-specific effects, we calculated tau-deposit-derived network using an alternative publicly available rs-fMRI database [human connectome project (HCP)] [38] . The cortical nodes identified in this analysis were similar to those derived with the GSP database (Fig. S5), supporting the robustness of our findings across different rs-fMRI datasets. And fourth, in order to ensure that the resultant networks were specific to the locations of tau deposit or atrophy, and not merely a reflection of hub regions in the brain, we contrasted the tau- and atrophy-network maps against the corresponding control maps generated with spatially randomized seed regions. The results were consistent with the original tau- and atrophy-network maps, confirming that the observed common networks were specifically derived from tau deposit and atrophy in PSP patients (Fig. S6).

Since it has been noted that tau deposits might cause neuronal loss and subsequent atrophy [6], one possible concern would be that the observed tau deposit-derived network might have partially reflected the remote effects of atrophy. To isolate tau-specific extended network, we further contrasted the tau- and atrophy-derived network maps. This analysis revealed cortical nodes with significantly stronger connectivity from the locations of tau deposit compared with atrophy, including the anterior dorsolateral PFC (adlPFC), pre-supplementary motor area (pre-SMA), dACC, premotor cortex (PMC), inferior frontal cortex (IFC), AI, and PPC ($p < 0.05$, FWE-corrected; Fig. 3C and F). Importantly, no regions showed the opposite, significantly stronger connectivity from the

locations of atrophy compared with tau deposits. We refer to this cortical network derived specifically from tau deposit as the PSP-tau network.

To assess whether the derived PSP-tau network corresponds to specific canonical functional networks in healthy subjects, we mapped regions in the PSP-tau network onto 12 functional networks defined in Ji et al. [39] (Fig. 3G). The distribution of regions across the networks were significantly uneven ($p < 1.0\times10^{-16}$, Chi-squared test), with the majority of regions assigned to the cingulo-opercular (action-mode) [40] network (CON: 66%), followed by the frontoparietal (FPN, 29%) and the language (LAN, 5.3%) networks. Nodes in none of the other nine networks (orbito-affective, ventral multimodal, posterior multimodal, default mode, auditory, dorsal attention, somatomotor, primary visual, and secondary visual networks) were included in the PSP-tau network (Fig. 3H). These results suggest that the cortical remote dysfunction caused predominantly by subcortical tau deposition in PSP patients is primarily linked to specific networks, especially CON and FPN.

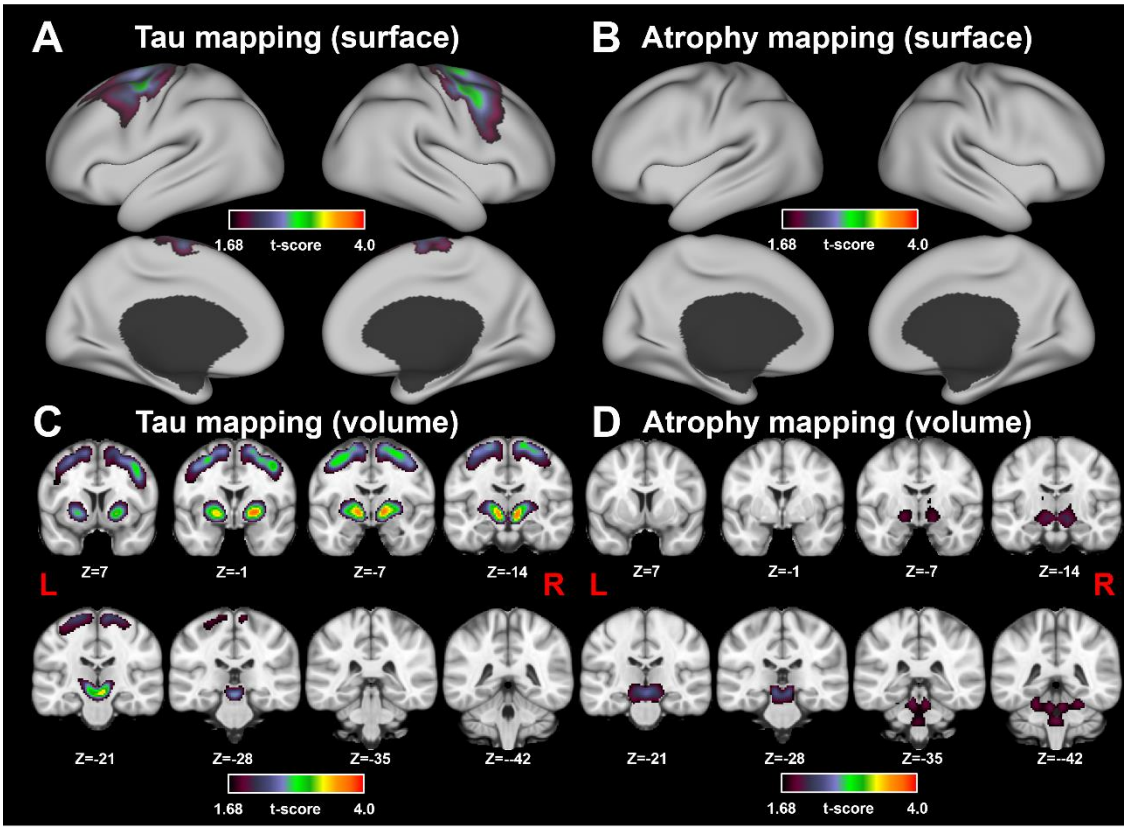

Fig. 2 Mean *t*-score maps of tau deposition (A, C) and atrophy (B, D) among PSP patients were presented on the surface (A, B) and volume space (C, D). Tau deposits were primarily observed subcortically in GP and midbrain. Moderate accumulation of tau was also detected in motor-related cortical areas in the precentral gyrus. Brain atrophy was observed in midbrain and cerebellum. Unpaired *t*-test was conducted against healthy controls.

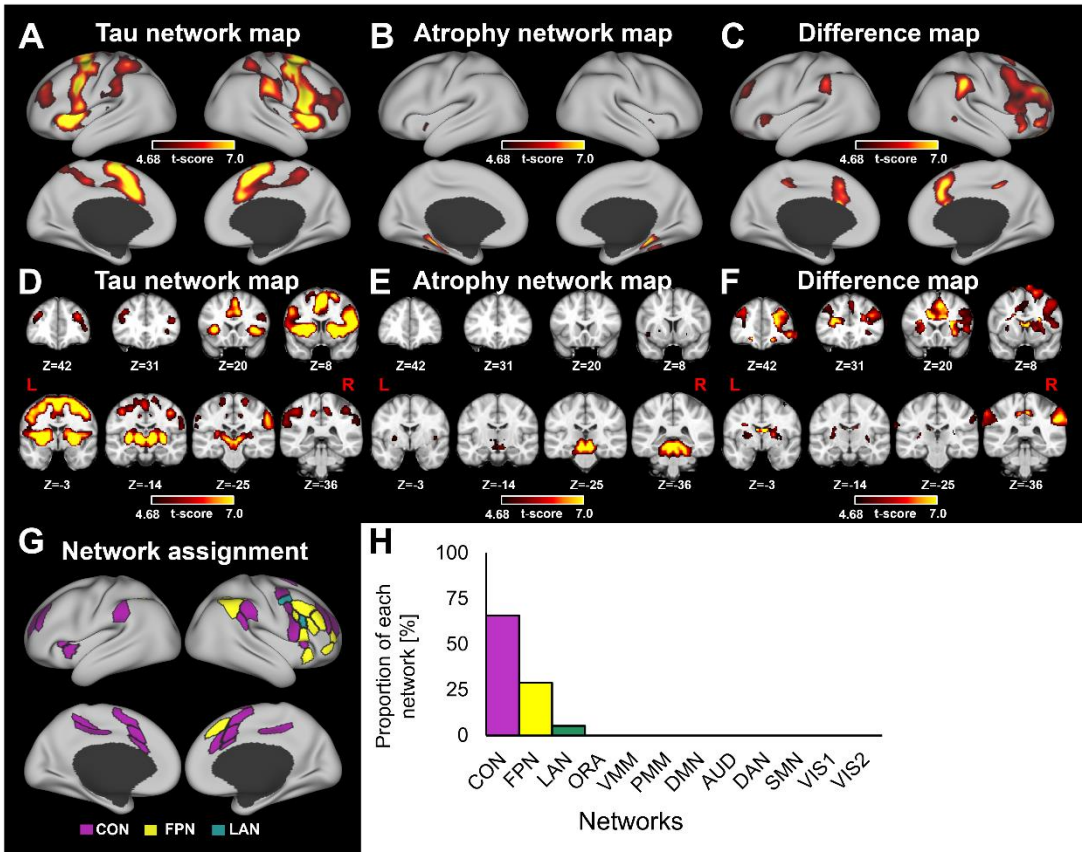

Fig. 3 Tau- and atrophy-network mapping for PSP patients. Average network maps calculated using tau deposit and atrophy VOIs among patients were presented on the surface (A and B for tau and atrophy, respectively) and volume space (D and E for tau and atrophy, respectively). *t*-score maps were obtained by comparing FC maps of tau deposit seeds vs. atrophy seeds (C, and F). Based on the cortical parcellation created by Ji et al., 2019, one of twelve networks was assigned to each region in the difference map (G), and proportion of each network area in the total area (38 areas) was calculated (H). CON: Cingulo-opercular network; FPN: Frontoparietal network; LAN: Language network; ORA: Orbito-affective network; VMM: Ventral multimodal network; PMM: Posterior multimodal network; DMN: Default mode network; AUD: Auditory network; DAN: Dorsal attention network; SMN: Somatomotor network; VIS1: Visual network 1; VIS2: Visual network 2.

FC between the locations of tau deposit and the PSP-tau network explained across-patient variability in the frontal cognitive declines

To examine the involvement of the PSP-tau network in a specific clinical symptom at the single-patient level, we examined the relationship between FC value from tau deposition sites to the PSP-tau network and clinical scores in the same patients. As a control analysis, we first examined the correlation between clinical scores and the degree of tau deposit/atrophy in the top two representative regions. The total score of PSPRS was significantly correlated with the degree of atrophy both in the midbrain ($p < 0.03$) and cerebellum ($p < 0.05$) (Fig. 4B). Of the subscores of PSPRS, the degrees of deficit in eye- and limb-movement were significantly correlated with the degree of tau deposit in the GP ($p < 0.006$) /midbrain ($p < 0.05$) (Fig. 4A), and atrophy in the midbrain ($p < 0.04$) (Fig. 4B), respectively. However, neither the above degrees of tau accumulation/atrophy significantly explained the variance in the score of Frontal Assessment Battery (FAB) [4], a general clinical test for measuring cognitive functions of the frontal cortex (Fig. 4A and B).

In contrast, the FC value between the locations of tau deposit and the PSP-tau network significantly anti-correlated with the score of FAB ($p < 0.04$), but not with any of the above motor-related clinical scores ($p > 0.9$) (Fig. 4C and E). Meanwhile, neither the above values of FC nor tau accumulation/atrophy significantly explained the variance in the degree of more general cognitive abilities [Mini-Mental State Examination (MMSE), $p > 0.1$)], apathy (Apathy Scale, $p > 0.3$), or depression [Geriatric Depression Score (GDS), $p > 0.1$]. To map the brain regions whose FC values with the locations of tau deposit predominantly explained the frontal cognitive impairments compared to motor symptoms, we created a contrast map between correlations of the FC value with the frontal cognitive- and motor-scores (Fig. 4D). After calculating correlation maps using the FAB total score and subscores for frontal cognitive impairments, and PSPRS total score and subscores for motor impairments, the scores that were the best explained by the FC value were adopted for each of frontal cognitive and motor symptoms. As a result, the total score of FAB, and a PSPRS subscore of limb movement deficit were used as indices for the frontal cognitive and motor impairments, respectively. The brain areas whose FC values with the locations of tau deposit predominantly explained the frontal cognitive deficits were adlPFC, dACC, premotor cortex, IFC, AI, and PPC (Fig. 4D), and were well consistent with the PSP-tau network (Fig. 4F: same as Fig. 3C).

More specifically, subscores of conceptualization and Go/NoGo in the FAB significantly anti-correlated with the FC value between the locations of tau deposit and

the PSP-tau network ($p < 0.005$ and 0.04 for conceptualization and Go/NoGo, respectively) (Fig. 4C). In the PSP-tau network, FC value to the Pre-SMA and AI best ($p < 0.007$) and worst ($p > 0.1$) explained the across-patient variance in the FAB total score, respectively (Fig. S7). To visualize the most relevant clinical score for each area in the PSP-tau network, we created a clinical score map by assigning the score showing the highest correlation or anti-correlation with the FC value from the locations of tau deposit (Fig. 4G) [Correlation maps between the FC value and each of the six clinical scores (PSPRS: total score, eye-movement, limb-movement; FAB: total score, conceptualization, Go/NoGo) were presented in Fig. S8]. Over 80% of areas in the PSP-tau network exhibited the highest correlation with the FAB-related cognitive scores. Together, these results suggest that, at the single-patient level, while the motor symptoms result directly from the local effects of subcortical tau deposits or atrophy, the frontal cognitive symptoms can be best explained as the remote effects of tau deposits exerted via the derived cortical PSP-tau network.

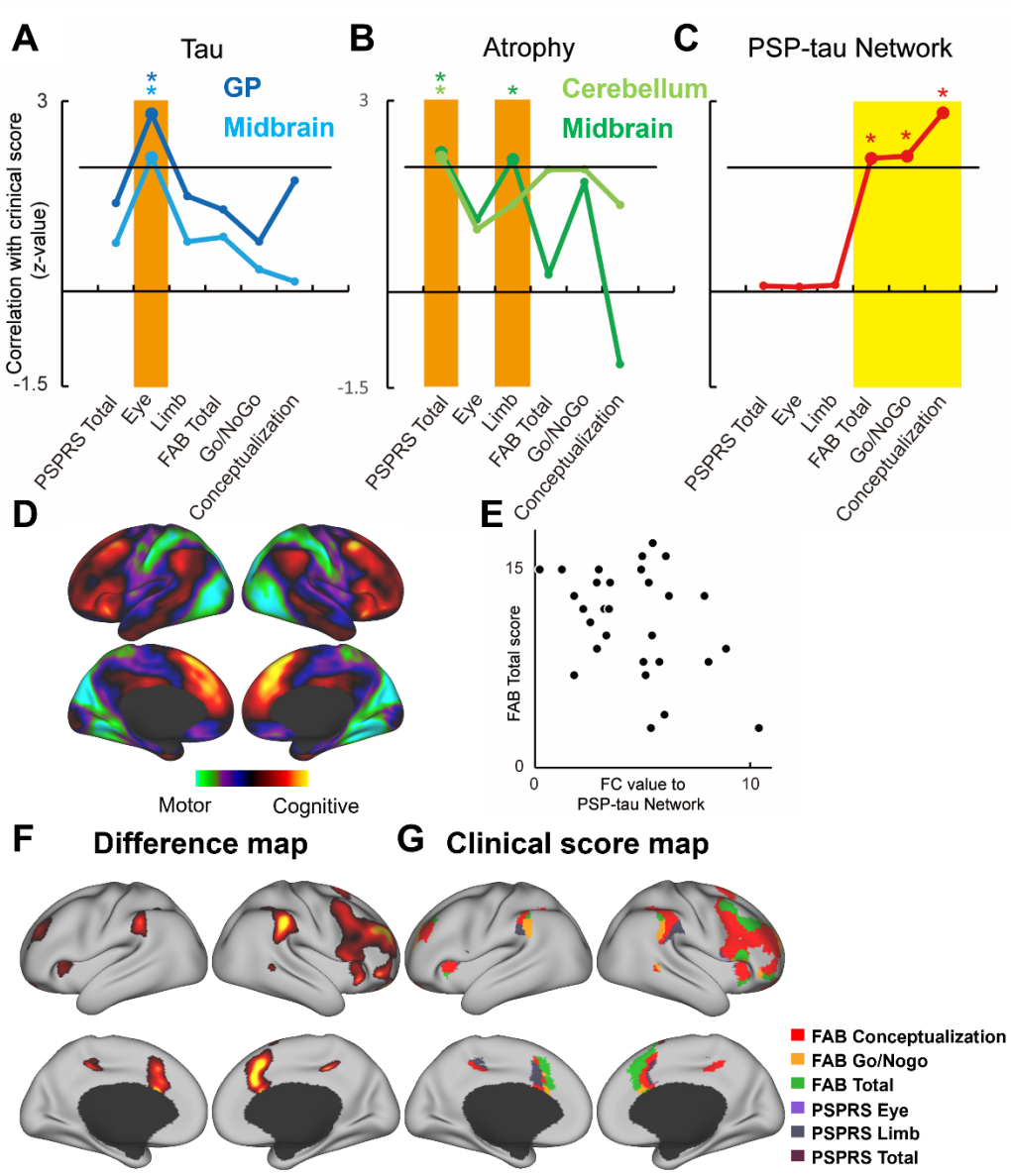

Fig. 4 Subcortical tau deposit/atrophy and the FC to tau-derived PSP network predict motor and frontal cognitive scales, respectively. Correlation between subcortical tau deposit (A) /atrophy (B), and FC from the tau deposits to the tau-derived PSP network (C) and motor/cognitive clinical scores. Black horizontal line, *z*-value at statistical threshold (p = 0.05). Orange and yellow boxes with asterisk, significant correlation for motor and cognitive clinical scores, respectively. Dark and light blue in the left panel, degree of tau deposit in the GP and midbrain, respectively. Dark and light green in the middle panel, degree of atrophy in the midbrain and cerebellum, respectively. Brain maps showing the regions having FC values explaining motor (PSPRS limb) or frontal cognitive (FAB total score) dysfunction (D). The FC values from the tau deposits to the tau-derived PSP network and the FAB total scores were negatively correlated with FAB total scores (E). The clinical scores with the strongest correlation were assigned to the

brain regions significantly different between tau and atrophy network mapping (F: same as Fig. 3C) using winner-take-all method (G).

DISCUSSION

We here conducted tau/atrophy-network mapping for PSP patients based on their tau deposits and atrophy mapped by multimodal imaging with a tau PET using a recently developed high-contrast tracer florzolotau and structural MRI. While the tau deposit and atrophy were predominantly detected in subcortical regions, the derived PSP-tau network was predominantly distributed across the canonical cortical networks of CON and FPN. This network was derived specifically from tau deposit, but not from atrophy. Critically, while the across-patient variance in the motor symptoms was significantly explained directly by local effects of tau deposit or atrophy in subcortical regions, the frontal cognitive symptoms were significantly explained only by the remote effects of tau deposits at the cortical PSP-tau network. These results suggest that the effects of tau deposits in heterogeneous regions across PSP patients remotely converge onto the cortical PSP-tau network, and this cortical convergence specifically well explained the frontal cognitive domain of their symptoms, which cannot be explained by local effects of subcortical tau deposits or atrophy.

Network mapping with normative rs-fMRI data of a large population of healthy subjects has been extensively conducted with brain lesions of stroke patients [41]. The present results demonstrate, for the first time, that this approach can be effectively extended to PET-detectable tau deposits in patients with a neurodegenerative disease. In particular, frontal cognitive, but not motor, domain of the clinical symptoms in individual PSP patients could be well explained by the FC values between the locations of tau deposit and the derived PSP-tau network, a proxy of the degree of remote effects exerted by tau deposits, whereas the degree of local tau deposit or atrophy in the subcortical regions with the maximum overlap across patients showed the opposite pattern, demonstrating the significance of the tau-network mapping for elucidating the brain-symptom relationships in tauopathy patients. The observations suggesting specific remote effects of tau deposit on a part of symptoms is consistent with the notion that seemingly cortical dysfunctions including the frontal cognitive deficits in PSP patients are not due directly to local tau deposits, but rather due to network effects remotely triggered by subcortical tau accumulations [20,22]. Despite that the current approach of tau-network mapping itself did not specifically focus on cognitive deficits, the resultant FC values between the locations of tau-deposit and the derived PSP-tau network explained some frontal cognitive aspects of clinical scores instead of more general severity of the disease measured by the total score of PSPRS or general cognitive abilities indexed by MMSE. It might be due partly to the fact that the derived PSP-tau network remote from tau deposits was predominantly composed of regions in the frontal cortex. The total score of

PSPRS was rather directly correlated with the degree of atrophy in the midbrain and cerebellum, which was consistent with previous studies [42].

Locations of tau deposit across patients with PSP were not entirely heterogeneous, but was partially overlapped, especially in the GP and midbrain. Indeed, these regions have been shown to exhibit significant positive FC and direct/indirect anatomical connectivity with some regions in the derived PSP-tau network [20,43]. This might raise a concern that the observed cortical pattern of common PSP-tau network is merely the reflection of FCs with a specific primary region of tau deposit. However, correlation with clinical scores showed totally different patterns between the degree of tau deposits in each of these regions and the FC value from the locations of tau deposit to the PSP-tau network, suggesting that the derived PSP-tau network was not merely a simple reflection of the FC pattern from a specific single brain region showing overlapped tau depositions across patients, but instead it presumably reflected FCs from multiple nodes where tau deposits distributed heterogeneously across the patients.

While the tau-network mapping provided a prominent pattern of convergent network, atrophy-network mapping for the same patients did not, across a range of statistical thresholds for defining seed regions. The results demonstrate the advantage of using tau deposit detected by florzolotau PET instead of atrophy captured by structural MRI to map the estimated remote effects of brain damages and to clarify the brain-symptom relationships in PSP. Tau deposition itself would be toxic to neurons directly or indirectly, and thus would lead to neuronal dysfunctions even without atrophy. Note that atrophy network mapping itself has been successfully conducted in previous studies including those for more large cohorts of patients with Alzheimer's disease [31] or schizophrenia[44]. In the current study, local degree of both tau deposition and atrophy significantly explained motor-related symptoms with a similar sensitivity, denying the possibility of critical difference in the data quality between the maps of tau deposit and atrophy themselves. However, it cannot be ruled out that more elaborated analysis of structural MRI data including normative modeling [45] with more large cohort might improve the resultant atrophy-network map in future study.

Previous studies have shown significant changes in the functional or anatomical connectivity in PSP patients. In particular, cortico-subcortical FC changes including those between the midbrain/thalamus and cortical areas have been reported for PSP patients [20,46]. Cortical targets of such FC changes partially overlap with the currently identified PSP-tau network. Furthermore, significant hypoperfusion and hypometabolism in PSP patients have been detected in the dACC, midcingulate cortex, and dlPFC [24,47,48], which are close to a part of nodes in the PSP-tau network. Therefore, these physiological

changes observed in PSP patients might be at least partly explained by the network we found in the present study based on the map of tau acccumulation in individual patients.

The derived PSP-tau network was predominantly overlapped with cingulo-opercular network, (also known as action mode network) [40,49]. This network is associated with planning, execution, monitoring, stopping of action, and attentional allocation based on both the top-down regulation and bottom-up sensory inputs. In the present study, FC values between regions with tau deposit and the derived PSP-tau network in individual patients were significantly anti-correlated with the FAB total score and its subscores including a Go/NoGo task (Fig. 4), consistent with the role for the network in stopping of a planned action. In particular, a deficit in response inhibition is one of primary symptoms in the PSP [50,51], and is likely reflected in the declined performance of a Go/NoGo task. Indeed, a majority of areas in the PSP-tau network are recruited in tasks requiring response inhibition [52], consistent with the currently observed relationships between the degree of suggested remote dysfunction of the PSP-tau network and the declined performance of a Go/NoGo task at the single-patient level.

The present study did not causally examine whether subcortical tau depositions indeed affect the functions of cortical PSP-tau network or whether the dysfunction of PSP-tau network indeed leads to, in particular, frontal cognitive symptoms. Recently, it has become possible to manipulate neural activity in nonhuman primates using chemogenetic techniques such as Designer Receptors Exclusively Activated by Designer Drugs (DREADDs) and Pharmacologically Selective Actuator Module / Pharmacologically Selective Effector Molecule (PSAM/PSEM) systems [53,54], and remote effects of neuronal silencing have been visualized at the functionally connected regions with behavioral relevance [55,56]. Therefore, causal validation and mechanistic understanding of the tau-network mapping via interventional experiments in non-human primate models would be one of intriguing directions for future research.

Other major limitations of the present study are as follows. First, although within-cohort reproducibility of the PSP-tau network was confirmed in a control analysis, its validation across independent cohorts would be required for more rigorous test of reproducibility. Another limitation is the cross-sectional design of the research. Longitudinal study of the tau-PET and tracking changes in the PSP-tau network in association with the assessment of symptom progression would lead to more causal understanding of the relationships between the tau-network map and the frontal cognitive symptoms. Another possibility of causal analysis is to test the effects of neuromodulation targeting a node in the PSP-tau network on the resultant relief from the frontal cognitive

symptoms. It would lead to a novel treatment option against this disease relying on biological evidence.

The present study demonstrated that tau-network mapping could identify a common cortical network with which tau deposition sites across PSP patients functionally connected. This reveals that the information of tau-PET images obtained from PSP patients can be applied to identify the relationships linking among the predominantly subcortical tau deposits, remote dysfunction of the connected cortical networks, and the resultant frontal cognitive symptoms in individual patients with the aid of normative connectome. The current approach would provide a potential target of neuromodulation for symptom-specific treatment in PSP patients, and might inform the future risk of frontal cognitive decline for patients in the early phase based on still subthreshold amount of tau deposits at brain regions connected with the PSP-tau network. Furthermore, this approach would be also widely appliable to other tauopathies including traumatic brain injury [57], late-onset psychiatric disorders, Alzheimer's disease, for which tau deposits can be detected with florzolotau, and other proteinopathies such as α-synucleinopathies [58], or other PET ligands measuring synaptic density or inflammation to understand the mediating networks between the PET-detectable local structural/functional changes and the resultant symptoms in a range of brain diseases.

MATERIALS AND METHODS

Participants

Forty-six patients with PSP-Richardson syndrome (PSP-RS) and 50 healthy controls (HCs) aged older than 40 years, without histories of neurological disorders were recruited from our affiliated hospitals and the volunteer association of our institute, respectively. The details of patient information were described in our previous paper [36], but PSP participants with PSP-tau score [36] of less than 0.3 and HCs with PSP-tau score of more than 0.1 were excluded from the later analyses. Final number of participants included were 37 and 48 for PSP patients and HCs, respectively. The participants underwent several neurological examinations, including PSPRS, FAB, MMSE, Apathy Scale, and GDS.

PET and MRI data acquisition and preprocessing

Florzolotau PET images were acquired to detect tau deposits using Biograph mCT flow system (Siemens, Erlangen, Germany) with 2 mm isotropic voxels. T1-weighted images (T1w) were acquired using 3T MRI scanner (MAGNETOM Verio, Siemens, Erlangen, Germany) for registration of PET images to the standard MRI space and evaluating the atrophy (repetition time [TR] = 2300 ms; echo time [TE] = 1.95 ms; inversion time [TI] = 900 ms; flip angle = 9°; field of view [FOV] = 250mm; matrix size = 512×512×176; slice thickness = 1 mm). The details of preprocessing were described in our previous paper [36]. Briefly, standardized uptake value ratio (SUVR) images were generated from averaged PET images with motion correction at the intervals of 90 – 110 min after intravenous injection of ^{18}F-florzolotau (186 ± 8.4 [MBq]). Individual SUVR images were spatially normalized to the standard Montreal Neurological Institute (MNI) space (East Asian brain T1w image from the International Consortium for Brain Mapping) using Diffeomorphic Anatomical Registration Through Exponentiated Lie Algebra (DARTEL) algorithm of the Statistical Parametric Mapping software (SPM12, Wellcome Department of Cognitive Neurology) on MATLAB (MathWorks).

Tau-network mapping

Tau-network mapping is an approach based on the lesion-network mapping that identifies brain regions functionally connected to lesion locations not using rs-fMRI scans of the participants themselves, but instead using a large-scale open database of rs-fMRI acquired from healthy subjects. In this study, FC maps were computed using rs-fMRI data obtained from 100 healthy subjects [25] in Brain Genomics Superstruct Project (GSP) [37] with the locations of tau deposit in individual patients as seed regions. Figure S1 shows the

analytical pipeline for tau-network mapping. In the first step, the regions of tau deposit for each PSP patient were identified by comparing with tau PET images of healthy controls. The *t*-score maps for individual patients were thresholded at $p < 0.001$ (two-sided, uncorrected), and were binarized to create the volume of interests (VOIs) for calculating FC maps. Next, the mean timeseries in the locations of tau deposits for each rs-fMRI data were compared with timeseries in every voxels to calculate the correlation maps. These maps for all 100 rs-fMRI datasets were combined to calculate the *t*-score map for each PSP patient. As a control condition of tau network mapping, we also calculated *t*-score maps using pseudo randomized VOIs. Briefly, ten voxels for each PSP patient (total 370 voxels) were randomly selected in the brain. *t*-score maps were then calculated using these pseudo randomized VOIs in the same manner as the original *t*-score maps for tau deposits. Finally, random control-subtracted tau-derived FC map was obtained by contrasting between the FC maps derived from tau deposits and randomized seeds. FC map calculation, statistical test, and surface mapping were performed using FMRIB Software Library's (FSL's) FEAT tool [59], Analysis of Functional NeuroImages (AFNI) software [60], and Connectome Workbentch [61], respectively.

Atrophy-network mapping

Data preprocessing for VBM was performed using SPM12 on MATLAB and PMOD 4.2 / 4.3 (PMOD Technologies LLC, Switzerland). Gray and white matter segmentation images were extracted from T1w images and were combined to obtain the parenchymal image using SPM12. The DARTEL algorithm was then employed to spatially normalize each brain parenchymal image (gray and white matter) by preserving amounts in MNI space. The regions of atrophy for each patient were identified by comparing with parenchymal images of healthy controls. The *t*-score maps for each patient were thresholded at $p < 0.001$ (two-sided, uncorrected), and were binarized to create the ROIs for calculating FC maps. Later analyses were the same as those in the tau network mapping described above.

Assignments of canonical networks to the derived PSP-tau network

Based on the atlas created by Ji et al. [39], one of twelve canonical networks including orbito-affective, ventral multimodal, posterior multimodal, default mode, auditory, frontoparietal, language, dorsal attention, cingulo-opercular (action-mode [40]), somatomotor, primary and secondary visual networks was assigned to each brain area in the derived PSP-tau network, which was determined as significant ($p < 0.05$, FWE-corrected) regions in a statistical comparison (paired *t*-test) between the FC maps derived

from tau- and atrophy-network mapping among the patients. The proportion of each network among 38 areas in the PSP-tau network was then calculated and its unevenness was statistically evaluated with the Chi-square test.

Validation analyses of tau/atrophy-network mapping

To determine the seed region for tau/atrophy network mapping, a statistical threshold of $p < 0.001$ (uncorrected) was adopted to identify the locations of significant tau deposition or atrophy in the PSP patients compared with the healthy controls. To examine the consistency/stability of the tau/atrophy-network mapping results among different criteria for the seed definition, both of more liberal ($p < 0.005$ uncorrected) and stringent ($p < 0.05$ FWE) thresholds were additionally used to identify the locations of tau deposition or atrophy in the PSP patients. Then, the resultant tau/atrophy-network maps were compared among the three different criteria. To confirm the reproducibility of tau/atrophy network mapping in the current cohort of PSP patients, tau-network maps calculated for individual patients (N = 37) were randomly divided into two groups. Then, FC values in the Johns Hopkins University (JHU) whole brain VOIs were compared between the two groups. To confirm the consistency of tau-network mapping results among different cohorts of rs-fMRI database, we also performed tau-network mapping based on the Human Connectome Project (HCP) [38] data. For each PSP patient, the FC map seeded from the locations of tau deposition was calculated with the HCP young adult dataset (N = 98) in the same manner as the analysis with the GSP dataset described above. The voxels with top 10% FC values in the cortex were then extracted from the resultant tau-network maps based on GSP/HCP data for comparison between the two rs-fMRI datasets.

Across-patient correlation between clinical scores and FC values linking tau deposit with the PSP-tau network

To visualize the regions whose FC value with locations of tau deposit explained the frontal cognitive impairments compared to the motor-related dysfunction, we contrasted the map of correlation between the FC and the frontal cognitive symptom against that between the FC and the motor deficits. Total score of the FAB and limb deficit score of the PSPRS were used as indices representing the frontal cognitive and motor impairments, respectively. To assess the relationships between the clinical scores and the FC value (between the locations of tau deposition and each area in the PSP-tau network), we extracted the mean FC values (*t*-scores) in the whole PSP-tau network and its constituent seven clusters. These clusters were named adlPFC, PMC, IFC, dACC, Pre SMA, PPC, and AI based on a previous human cortical parcellation [62]. We also extracted the degree

of tau deposition and atrophy (*t*-scores as described above) in the top 2 regions, i.e., GP and midbrain for tau deposition, midbrain and cerebellum for atrophy, respectively. Pearson's correlation coefficient was then calculated between these values and clinical scores (PSPRS and FAB, including their subscores). The rest of clinical scores (i.e., MMSE, Apathy Scale, and GDS) were served as controls. Finally, the clinical scores with the strongest correlation were assigned to each brain region of the PSP-tau network. These analyses were performed using SPM12, Connectome Workbench, and FSL software.

References and Notes

1 Steele, J. C., Richardson, J. C. & Olszewski, J. Progressive Supranuclear Palsy. A Heterogeneous Degeneration Involving the Brain Stem, Basal Ganglia and Cerebellum with Vertical Gaze and Pseudobulbar Palsy, Nuchal Dystonia and Dementia. *Arch Neurol* **10**, 333-359 (1964). https://doi.org/10.1001/archneur.1964.00460160003001

2 Hauw, J. J. *et al.* Preliminary NINDS neuropathologic criteria for Steele-Richardson-Olszewski syndrome (progressive supranuclear palsy). *Neurology* **44**, 2015-2019 (1994). https://doi.org/10.1212/wnl.44.11.2015

3 Hoglinger, G. U. *et al.* Clinical diagnosis of progressive supranuclear palsy: The movement disorder society criteria. *Mov Disord* **32**, 853-864 (2017). https://doi.org/10.1002/mds.26987

4 Dubois, B., Slachevsky, A., Litvan, I. & Pillon, B. The FAB: a Frontal Assessment Battery at bedside. *Neurology* **55**, 1621-1626 (2000). https://doi.org/10.1212/wnl.55.11.1621

5 Donker Kaat, L. *et al.* Frontal presentation in progressive supranuclear palsy. *Neurology* **69**, 723-729 (2007). https://doi.org/10.1212/01.wnl.0000267643.24870.26

6 Ballatore, C., Lee, V. M. & Trojanowski, J. Q. Tau-mediated neurodegeneration in Alzheimer's disease and related disorders. *Nat Rev Neurosci* **8**, 663-672 (2007). https://doi.org/10.1038/nrn2194

7 Maruyama, M. *et al.* Imaging of tau pathology in a tauopathy mouse model and in Alzheimer patients compared to normal controls. *Neuron* **79**, 1094-1108 (2013). https://doi.org/10.1016/j.neuron.2013.07.037

8 Verny, M., Duyckaerts, C., Agid, Y. & Hauw, J. J. The significance of cortical pathology in progressive supranuclear palsy. Clinico-pathological data in 10 cases. *Brain* **119 (Pt 4)**, 1123-1136 (1996). https://doi.org/10.1093/brain/119.4.1123

9 Alster, P. *et al.* Accumulation of Tau Protein, Metabolism and Perfusion-Application and Efficacy of Positron Emission Tomography (PET) and Single Photon Emission Computed Tomography (SPECT) Imaging in the Examination of Progressive Supranuclear Palsy (PSP) and Corticobasal Syndrome (CBS). *Front Neurol* **10**, 101 (2019). https://doi.org/10.3389/fneur.2019.00101

10 Hauw, J. J. *et al.* Constant neurofibrillary changes in the neocortex in progressive supranuclear palsy. Basic differences with Alzheimer's disease and aging. *Neurosci Lett* **119**, 182-186 (1990). https://doi.org/10.1016/0304-3940(90)90829-x

11 Chen, Y. *et al.* Pathology-specific patterns of cerebellar atrophy in neurodegenerative disorders. *Alzheimers Dement* **20**, 1771-1783 (2024). https://doi.org/10.1002/alz.13551

12 Price, S. *et al.* Voxel-based morphometry detects patterns of atrophy that help differentiate progressive supranuclear palsy and Parkinson's disease. *Neuroimage* **23**, 663-669 (2004). https://doi.org/10.1016/j.neuroimage.2004.06.013

13 Josephs, K. A. *et al.* Voxel-based morphometry in autopsy proven PSP and CBD. *Neurobiol Aging* **29**, 280-289 (2008). https://doi.org/10.1016/j.neurobiolaging.2006.09.019

14 Boxer, A. L. *et al.* Patterns of brain atrophy that differentiate corticobasal degeneration syndrome from progressive supranuclear palsy. *Arch Neurol* **63**, 81-86 (2006). https://doi.org/10.1001/archneur.63.1.81

15 Cope, T. E. *et al.* Tau burden and the functional connectome in Alzheimer's disease and progressive supranuclear palsy. *Brain* **141**, 550-567 (2018). https://doi.org/10.1093/brain/awx347

16 Seeley, W. W., Crawford, R. K., Zhou, J., Miller, B. L. & Greicius, M. D. Neurodegenerative diseases target large-scale human brain networks. *Neuron* **62**, 42-52 (2009). https://doi.org/10.1016/j.neuron.2009.03.024

17 Seeley, W. W. *et al.* Early frontotemporal dementia targets neurons unique to apes and humans. *Ann Neurol* **60**, 660-667 (2006). https://doi.org/10.1002/ana.21055

18 Graveland, G. A., Williams, R. S. & DiFiglia, M. Evidence for degenerative and regenerative changes in neostriatal spiny neurons in Huntington's disease. *Science* **227**, 770-773 (1985). https://doi.org/10.1126/science.3155875

19 Selkoe, D. J. Alzheimer's disease is a synaptic failure. *Science* **298**, 789-791 (2002). https://doi.org/10.1126/science.1074069

20 Gardner, R. C. *et al.* Intrinsic connectivity network disruption in progressive supranuclear palsy. *Ann Neurol* **73**, 603-616 (2013). https://doi.org/10.1002/ana.23844

21 Gurd, J. M. & Hodges, J. R. Word-retrieval in two cases of progressive supranuclear palsy. *Behav Neurol* **10**, 31-41 (1997). https://doi.org/10.3233/BEN-1997-10106

22 Roemer, S. N. *et al.* Subcortical tau is linked to hypoperfusion in connected cortical regions in 4-repeat tauopathies. *Brain* **147**, 2428-2439 (2024). https://doi.org/10.1093/brain/awae174

23 Whitwell, J. L. *et al.* Radiological biomarkers for diagnosis in PSP: Where are we and where do we need to be? *Mov Disord* **32**, 955-971 (2017). https://doi.org/10.1002/mds.27038

24 Salmon, E., Van der Linden, M. V. & Franck, G. Anterior cingulate and motor network metabolic impairment in progressive supranuclear palsy. *Neuroimage* **5**, 173-178 (1997). https://doi.org/10.1006/nimg.1997.0262

25 Boes, A. D. *et al.* Network localization of neurological symptoms from focal brain lesions. *Brain* **138**, 3061-3075 (2015). https://doi.org/10.1093/brain/awv228

26 Darby, R. R., Laganiere, S., Pascual-Leone, A., Prasad, S. & Fox, M. D. Finding the imposter: brain connectivity of lesions causing delusional misidentifications. *Brain* **140**, 497-507 (2017). https://doi.org/10.1093/brain/aww288

27 Ferguson, M. A. *et al.* A human memory circuit derived from brain lesions causing amnesia. *Nat Commun* **10**, 3497 (2019). https://doi.org/10.1038/s41467-019-11353-z

28 Fischer, D. B. *et al.* A human brain network derived from coma-causing brainstem lesions. *Neurology* **87**, 2427-2434 (2016). https://doi.org/10.1212/WNL.0000000000003404

29 Darby, R. R., Horn, A., Cushman, F. & Fox, M. D. Lesion network localization of criminal behavior. *Proc Natl Acad Sci U S A* **115**, 601-606 (2018). https://doi.org/10.1073/pnas.1706587115

30 Laganiere, S., Boes, A. D. & Fox, M. D. Network localization of hemichorea-hemiballismus. *Neurology* **86**, 2187-2195 (2016). https://doi.org/10.1212/WNL.0000000000002741

31 Tetreault, A. M. *et al.* Network localization of clinical, cognitive, and neuropsychiatric symptoms in Alzheimer's disease. *Brain* **143**, 1249-1260 (2020). https://doi.org/10.1093/brain/awaa058

32 Padmanabhan, J. L. *et al.* A Human Depression Circuit Derived From Focal Brain Lesions. *Biol Psychiatry* **86**, 749-758 (2019). https://doi.org/10.1016/j.biopsych.2019.07.023

33 Joutsa, J. *et al.* Brain lesions disrupting addiction map to a common human brain circuit. *Nat Med* **28**, 1249-1255 (2022). https://doi.org/10.1038/s41591-022-01834-y

34 Tagai, K. *et al.* High-Contrast In Vivo Imaging of Tau Pathologies in Alzheimer's and Non-Alzheimer's Disease Tauopathies. *Neuron* **109**, 42-58 e48 (2021). https://doi.org/10.1016/j.neuron.2020.09.042

35 Tezuka, T. *et al.* Evaluation of [(18)F]PI-2620, a second-generation selective tau tracer, for assessing four-repeat tauopathies. *Brain Commun* **3**, fcab190 (2021). https://doi.org/10.1093/braincomms/fcab190

36 Endo, H. *et al.* A Machine Learning-Based Approach to Discrimination of Tauopathies Using [(18) F]PM-PBB3 PET Images. *Mov Disord* **37**, 2236-2246 (2022). https://doi.org/10.1002/mds.29173

37 Yeo, B. T. *et al.* The organization of the human cerebral cortex estimated by intrinsic functional connectivity. *J Neurophysiol* **106**, 1125-1165 (2011). https://doi.org/10.1152/jn.00338.2011

38 Van Essen, D. C. *et al.* The WU-Minn Human Connectome Project: an overview. *Neuroimage* **80**, 62-79 (2013). https://doi.org/10.1016/j.neuroimage.2013.05.041

39 Ji, J. L. *et al.* Mapping the human brain's cortical-subcortical functional network organization. *Neuroimage* **185**, 35-57 (2019). https://doi.org/10.1016/j.neuroimage.2018.10.006

40 Dosenbach, N. U. F., Raichle, M. E. & Gordon, E. M. The brain's action-mode network. *Nat Rev Neurosci* (2025). https://doi.org/10.1038/s41583-024-00895-x

41 Siddiqi, S. H., Kording, K. P., Parvizi, J. & Fox, M. D. Causal mapping of human brain function. *Nat Rev Neurosci* **23**, 361-375 (2022). https://doi.org/10.1038/s41583-022-00583-8

42 Dutt, S. *et al.* Progression of brain atrophy in PSP and CBS over 6 months and 1 year. *Neurology* **87**, 2016-2025 (2016). https://doi.org/10.1212/WNL.0000000000003305

43 Middleton, F. A. & Strick, P. L. Anatomical evidence for cerebellar and basal ganglia involvement in higher cognitive function. *Science* **266**, 458-461 (1994). https://doi.org/10.1126/science.7939688

44 Makhlouf, A. T. *et al.* Heterogeneous patterns of brain atrophy in schizophrenia localize to a common brain network. *Nature Mental Health* (2024). https://doi.org/https://doi.org/10.1038/s44220-024-00348-5

45 Segal, A. *et al.* Regional, circuit and network heterogeneity of brain abnormalities in psychiatric disorders. *Nat Neurosci* **26**, 1613-1629 (2023). https://doi.org/10.1038/s41593-023-01404-6

46 Piattella, M. C. *et al.* Disrupted resting-state functional connectivity in progressive supranuclear palsy. *AJNR Am J Neuroradiol* **36**, 915-921 (2015). https://doi.org/10.3174/ajnr.A4229

47 Chiu, W. Z. *et al.* Midcingulate involvement in progressive supranuclear palsy and tau positive frontotemporal dementia. *J Neurol Neurosurg Psychiatry* **83**, 910-915 (2012). https://doi.org/10.1136/jnnp-2011-302035

48 Varrone, A. *et al.* Identification by [99mTc]ECD SPECT of anterior cingulate hypoperfusion in progressive supranuclear palsy, in comparison with Parkinson's disease. *Eur J Nucl Med Mol Imaging* **34**, 1071-1081 (2007). https://doi.org/10.1007/s00259-006-0344-7

49 Dosenbach, N. U. *et al.* A core system for the implementation of task sets. *Neuron* **50**, 799-812 (2006). https://doi.org/10.1016/j.neuron.2006.04.031

50 Zhang, J. *et al.* Different decision deficits impair response inhibition in progressive supranuclear palsy and Parkinson's disease. *Brain* **139**, 161-173 (2016). https://doi.org/10.1093/brain/awv331

51 Migliaccio, R. *et al.* Cognitive and behavioural inhibition deficits in neurodegenerative dementias. *Cortex* **131**, 265-283 (2020). https://doi.org/10.1016/j.cortex.2020.08.001

52 Aron, A. R. & Poldrack, R. A. Cortical and subcortical contributions to Stop signal response inhibition: role of the subthalamic nucleus. *J Neurosci* **26**, 2424-2433 (2006). https://doi.org/10.1523/JNEUROSCI.4682-05.2006

53 Nagai, Y. *et al.* Deschloroclozapine, a potent and selective chemogenetic actuator enables rapid neuronal and behavioral modulations in mice and monkeys. *Nat Neurosci* **23**, 1157-1167 (2020). https://doi.org/10.1038/s41593-020-0661-3

54 Hori, Y. *et al.* Multimodal Imaging for Validation and Optimization of Ion Channel-Based Chemogenetics in Nonhuman Primates. *J Neurosci* **43**, 6619-6627 (2023). https://doi.org/10.1523/JNEUROSCI.0625-23.2023

55 Hirabayashi, T. *et al.* Chemogenetic sensory fMRI reveals behaviorally relevant bidirectional changes in primate somatosensory network. *Neuron* **109**, 3312-3322 e3315 (2021). https://doi.org/10.1016/j.neuron.2021.08.032

56 Hirabayashi, T. *et al.* Multiscale Chemogenetic Dissection of Fronto-temporal Top-down Regulation for Object Memory in Primates. *Nature Communications* (2024). https://doi.org/https://doi.org/10.1038/s41467-024-49570-w

57 Takahata, K. *et al.* PET-detectable tau pathology correlates with long-term neuropsychiatric outcomes in patients with traumatic brain injury. *Brain* **142**, 3265-3279 (2019). https://doi.org/10.1093/brain/awz238

58 Endo, H. *et al.* Imaging alpha-synuclein pathologies in animal models and patients with Parkinson's and related diseases. *Neuron* **112**, 2540-2557 e2548 (2024). https://doi.org/10.1016/j.neuron.2024.05.006

59 Smith, S. M. *et al.* Advances in functional and structural MR image analysis and implementation as FSL. *Neuroimage* **23 Suppl 1**, S208-219 (2004). https://doi.org/10.1016/j.neuroimage.2004.07.051

60 Cox, R. W. AFNI: software for analysis and visualization of functional magnetic resonance neuroimages. *Comput Biomed Res* **29**, 162-173 (1996). https://doi.org/10.1006/cbmr.1996.0014

61 Marcus, D. S. *et al.* Informatics and data mining tools and strategies for the human connectome project. *Front Neuroinform* **5**, 4 (2011). https://doi.org/10.3389/fninf.2011.00004

62 Glasser, M. F. *et al.* A multi-modal parcellation of human cerebral cortex. *Nature* **536**, 171-178 (2016). https://doi.org/10.1038/nature18933

Acknowledgments:
We thank all patients and their caregivers, as well as volunteers, for their participation in this study; clinical research coordinators; PET and MRI operators; radiochemists; and research ethics advisers at Quantum Science and Technology (QST) for their assistance with the current projects. We acknowledge the support of Matsuoka, K. Hirata, M. Oya, H. Matsumoto, M. Ichihashi, Y. Komatsu, Y. Yamamoto, M. Kubota, K. S. Kitamura, Y. Takado, K. Kawamura, and M.R. Zhang at QST. We thank APRINOIA Therapeutics for kindly sharing the precursor of florzolotau (18F). We acknowledge the support of S. Hirano and Y. Nakano at the Department of Neurology, Chiba University on patient recruitment; T. Hatano, T. Tsunemi, N. Nishikawa, K. Nishioka (currently working at The Juntendo Tokyo Koto Geriatric Medical Center), Y. Yamashita, Y. Motoi, and S. Saiki (currently working at the University of Tsukuba) at the Department of Neurology, Juntendo University School of Medicine; I. Aiba at the Department of Neurology, National Hospital Organization Higashinagoya National Hospital; T. Yuasa at the Department of Neurology, Kamagaya General Hospital; H. Imai at the Tokyo Rinkai Hospital; Y. Nishida and Y. Yagi at the Department of Neurology, Tokyo Medical and Dental University; S. Furukawa at the Narita Red Cross Hospital; M. Seki at the Department of Neurology, Keio University School of Medicine; and T. Takeda and I. Isose at the Department of Neurology, Chiba-East Hospital. Data were provided in part by the Human Connectome Project, WU-Minn Consortium (Principal Investigators: David Van Essen and Kamil Ugurbil; 1U54MH091657) funded by the 16 NIH Institutes and Centers that support the NIH Blueprint for Neuroscience Research; and by the McDonnell Center for Systems Neuroscience at Washington University.

Funding:
AMED Grant JP24wm0625307 (to TH)
AMED Grant JP19dm0207072 (to MH)
AMED Grant JP24wm0625001 (to MH)
JST Grant JPMJMS2024 (to MH)
MEXT/JSPS KAKENHI JP24H00734 (to TH)
MEXT/JSPS KAKENHI JP23K11796 (to YH)
Biogen Idec Inc.
APRINOIA Therapeutics.

Author contributions:

Conceptualization: TH
Methodology: YH, TH, HE
Investigation: YH, TH, HE
Visualization: YH, TH
Funding acquisition: TH, YH, HE, MH, TM
Project administration: TH
Supervision: TH, EH, TM, MH
Writing – original draft: YH, TH
Writing – review & editing: All authors

Competing interests:

H. Shimada, and M.H. hold patents on compounds related to this report.

Data and materials availability:

The data supporting our study findings are available from the corresponding author upon reasonable request.

Supplementary Figures

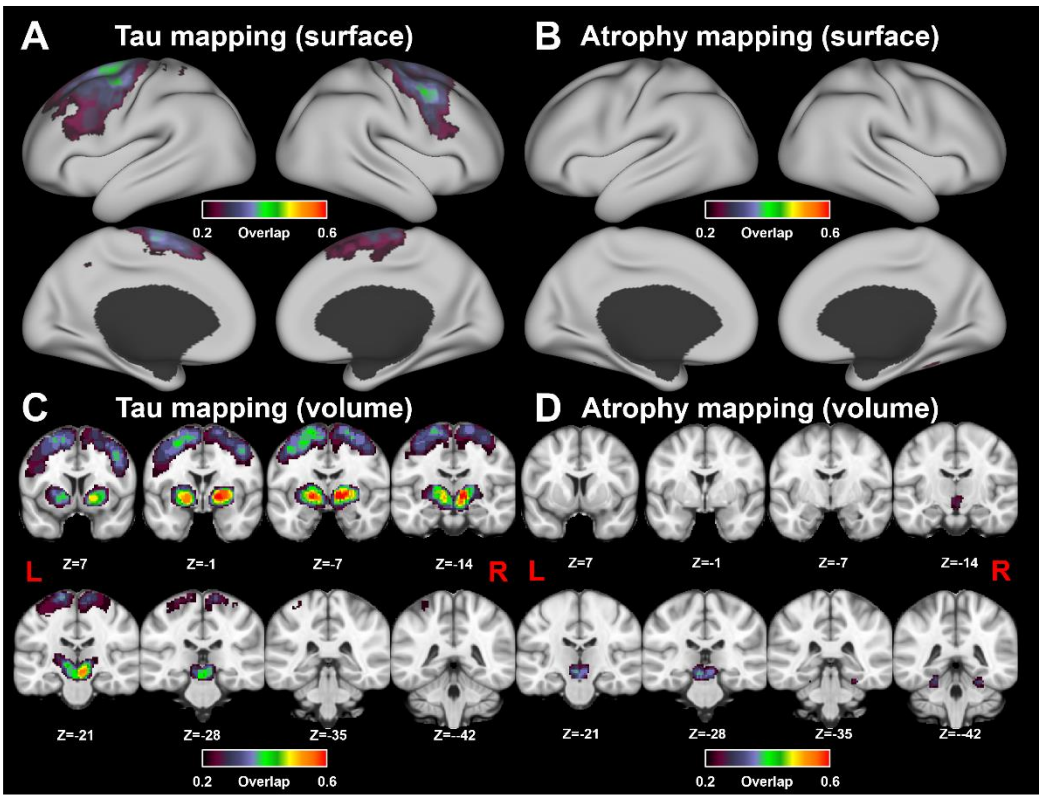

Fig. S1 Overlap of tau deposit and brain atrophy locations among PSP patients. Overlap maps for tau deposit (A, C) and atrophy (B, D) were presented on the surface (A, B) and volume space (C, D). Tau was accumulated in the GP (thresholded at $p < 0.001$, overlapped maximally for 62% of patients), thalamus (62%) and midbrain (57%), and parts of motor-related cortex (25%), while brain atrophy was observed in midbrain (35%) and cerebellum (32%).

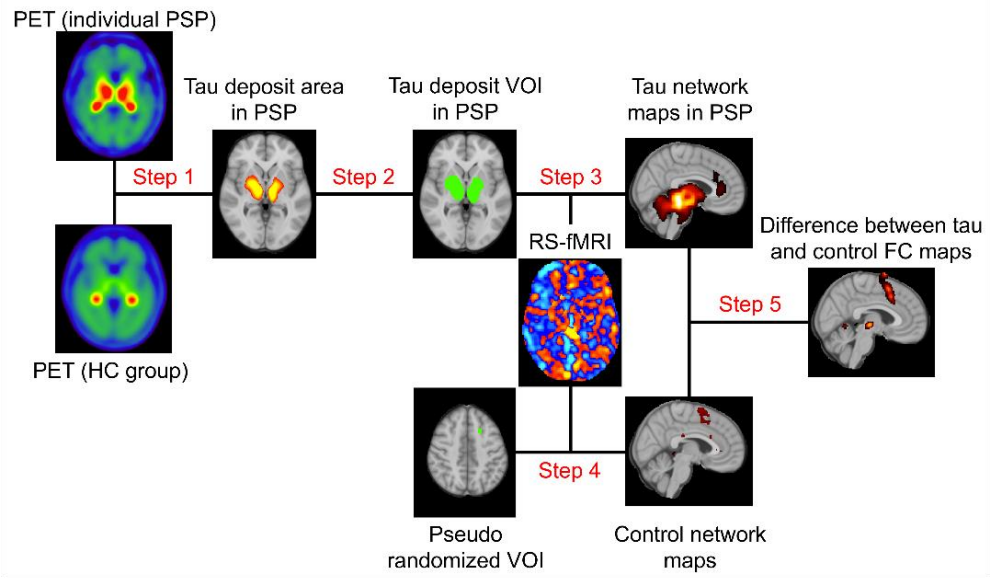

Fig. S2 Pipeline for tau network mapping. The areas of tau deposit for each PSP patient were identified by comparing with tau PET images of healthy controls (Step 1). The *t*-score maps were then thresholded by $p < 0.001$ (uncorrected), and binarized to create the VOIs (Step 2). Next, the mean timeseries in the VOI from each rs-fMRI data (n=100) were compared with timeseries for every voxel to calculate the correlation maps (tau network maps). These maps for all 100 rs-fMRI datasets were combined to calculate the *t*-score maps in each PSP patient (Step 3). As a control condition of tau network mapping, ten voxels for each PSP patient were generated by randomly selecting the position in the brain. *t*-score maps were calculated using pseudo randomized voxel in the same manner as tau deposit VOIs as described above (Step 4). Finally, tau-derived FC maps were obtained by calculating *t*-score maps between tau deposit and control FC maps (Step 5).

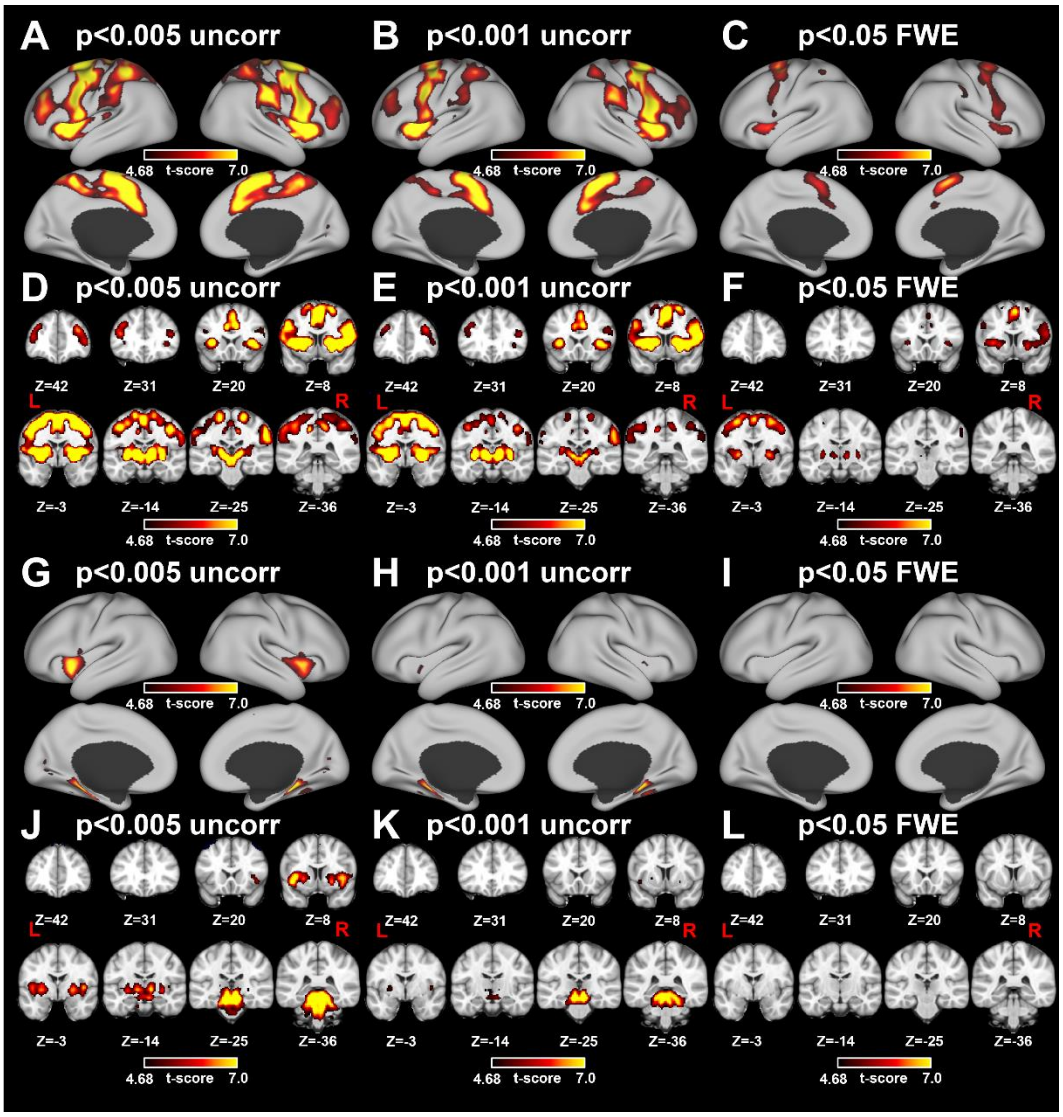

Fig. S3 Tau (A-F) and atrophy (G-L) network maps were obtained using local tau deposit and atrophied regions calculated by three different criteria ($p < 0.005$ uncorrected, $p < 0.001$ uncorrected, and $p < 0.05$ FWE corrected).

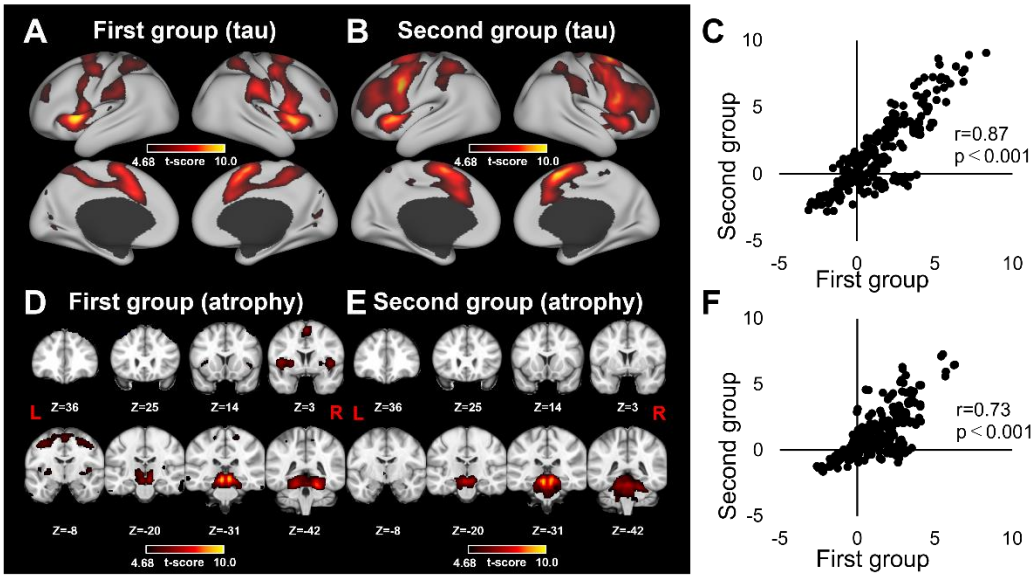

Fig. S4 Reproducibility of tau deposit and atrophy network mapping. Each map for split-half subgroups was presented on the surface for tau deposit maps (A for earlier and B for later patient number) and on the volume for atrophy maps (D for earlier and E for later patient number). The VOI values in the tau deposit (C) and atrophy maps (F) were well consistent between two groups (C, $r = 0.87$, $p < 0.001$; F, $r = 0.73$, $p < 0.001$).

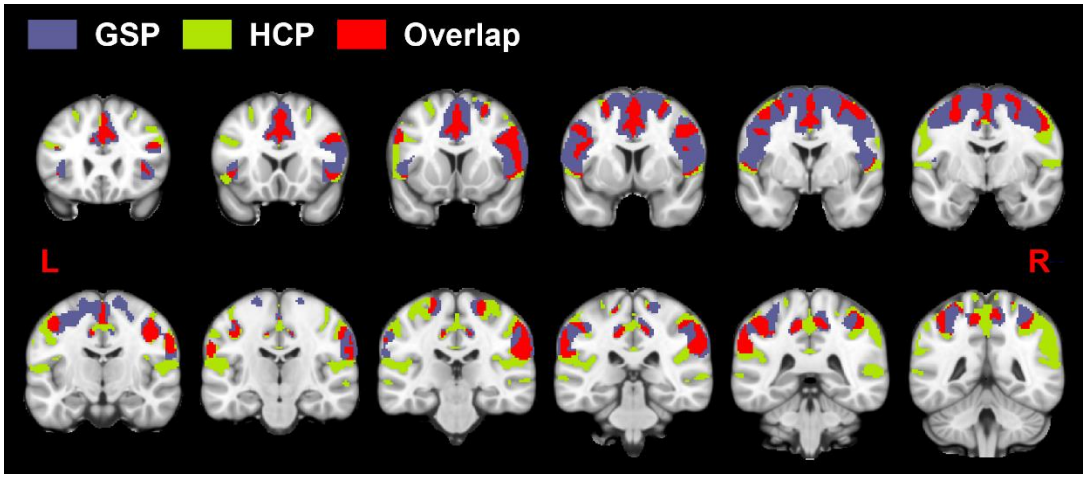

Fig. S5 Validation of tau network mapping. Tau network maps were computed from GSP and HCP database. The top 10% voxels of the FC values in the cortex are shown in blue (GSP) and green (HCP) regions. Overlap areas (red) between two cohorts are found in LFC, ACC, PPC, and AI.

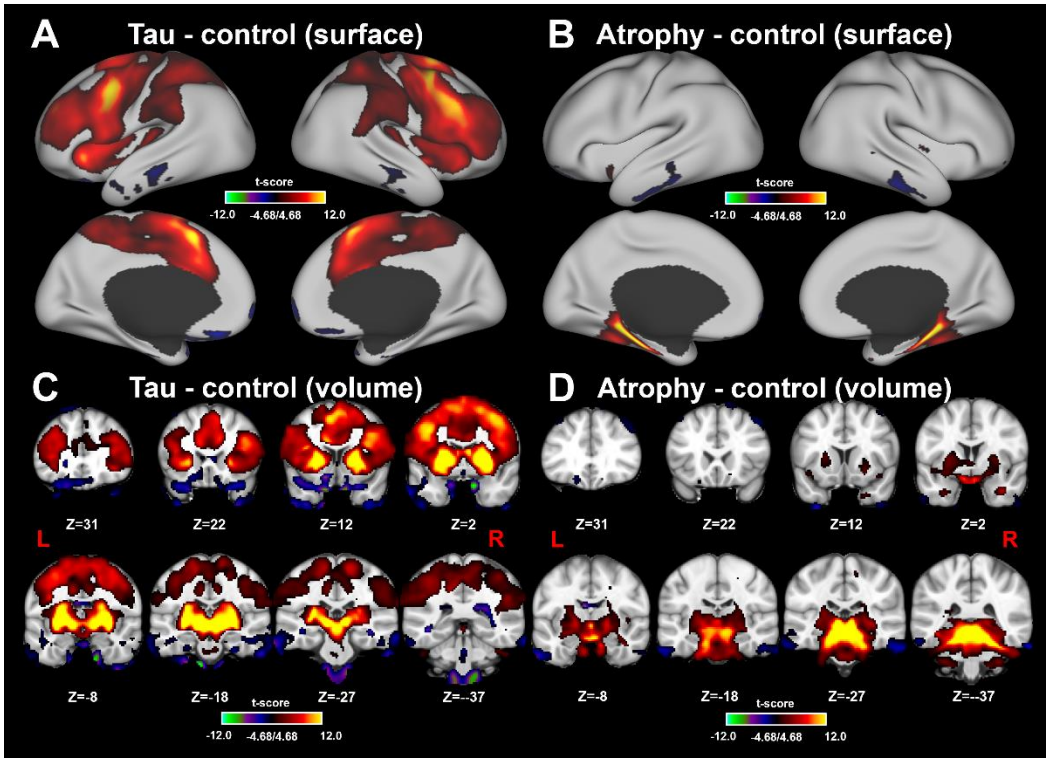

Fig. S6 Comparison of tau and atrophy maps with control FC maps calculated by pseudo randomized VOIs. T-score maps were presented on the surface (A for tau and B for atrophy) and volume space (C for tau and D for atrophy).

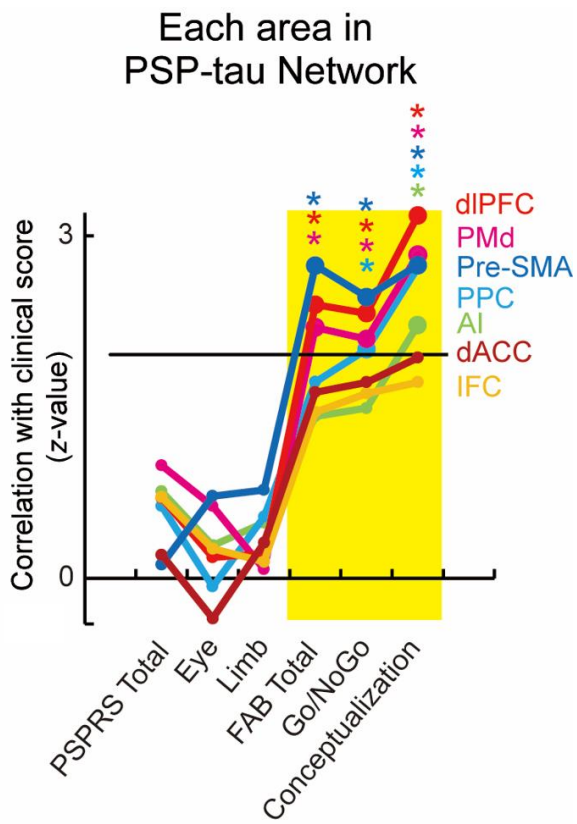

Fig. S7 Correlation between the FC from tau deposits to each area in the tau-derived PSP network and the score of clinical symptoms. Red, adlPFC; magenta, premotor cortex; blue, dACC; cyan, PPC; light green, AI. Black horizontal line, *z*-value at statistical threshold (p = 0.05). *, significant correlation.

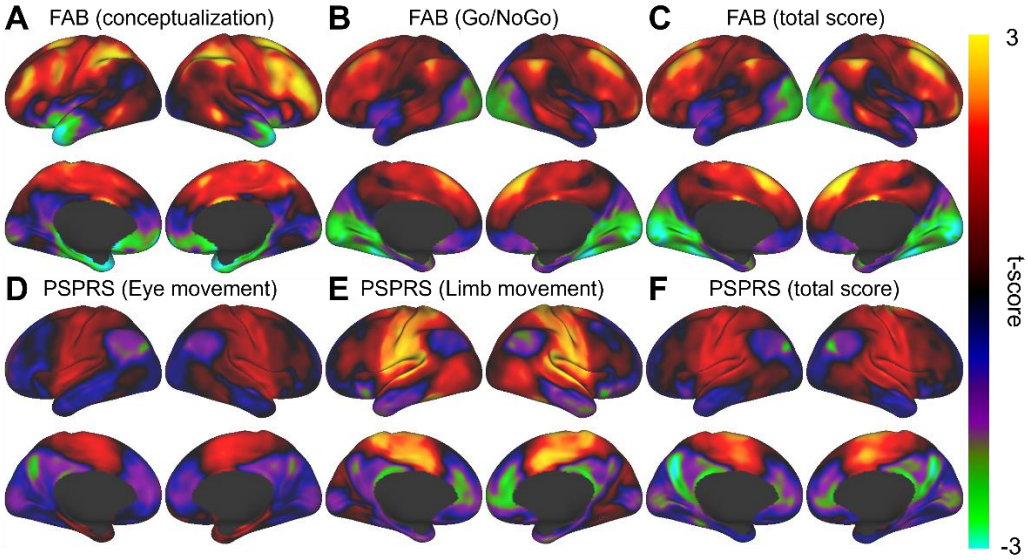

Fig. S8 Univariate correlation maps between FC maps seeded from tau deposits and the score of cognitive (A-C) and motor (D-F) symptoms.